Supplemental Figures

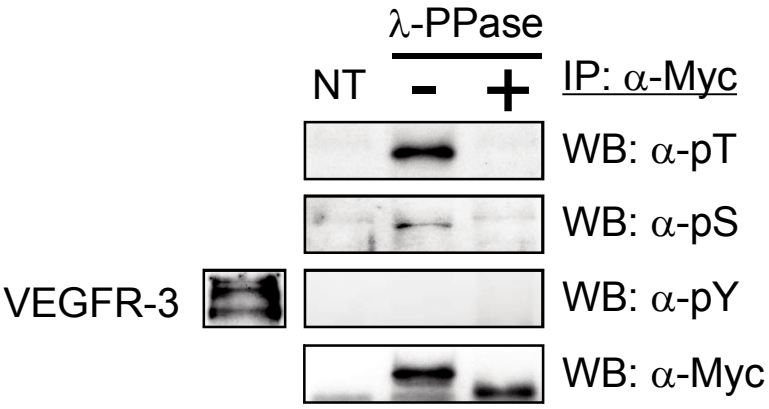

Supplemental Figure S1. **FOXC2 is phosphorylated on both serine and threonine but not on tyrosine residues.** Adenovirus-expressed Myc-FOXC2 was immunoprecipitated from HepG2 cells with anti-Myc antibody (IP: α-Myc) and treated (+) or not (-) with lambda protein phosphatase (λ-PPase) while the protein was still bound to the immunoaffinity beads. The immunoprecipitates were analyzed by Western blotting (WB) with anti-phosphothreonine (α-pT), anti-phosphoserine (α-pS), anti-phosphotyrosine (α-pY) and anti-Myc antibodies. Immunoprecipitate from non-transduced (NT) cells was used as a negative control. Tyrosine-phosphorylated vascular endothelial growth factor receptor 3 (VEGFR-3) was used as a positive control in the α-pY immunoblot. Disappearance of bands corresponding to the phosphatase-treated protein is diagnostic of phosphorylation and confirms the antibody specificity. Higher intensity of the α-pT band compared to that of the α-pS band is not due to predominant threonine phosphorylation, but rather to the higher quality of the α-pT antibody. The nonspecific band seen in the α-pS blot corresponds to the heavy chain of the α-Myc antibody used in immunoprecipitation.

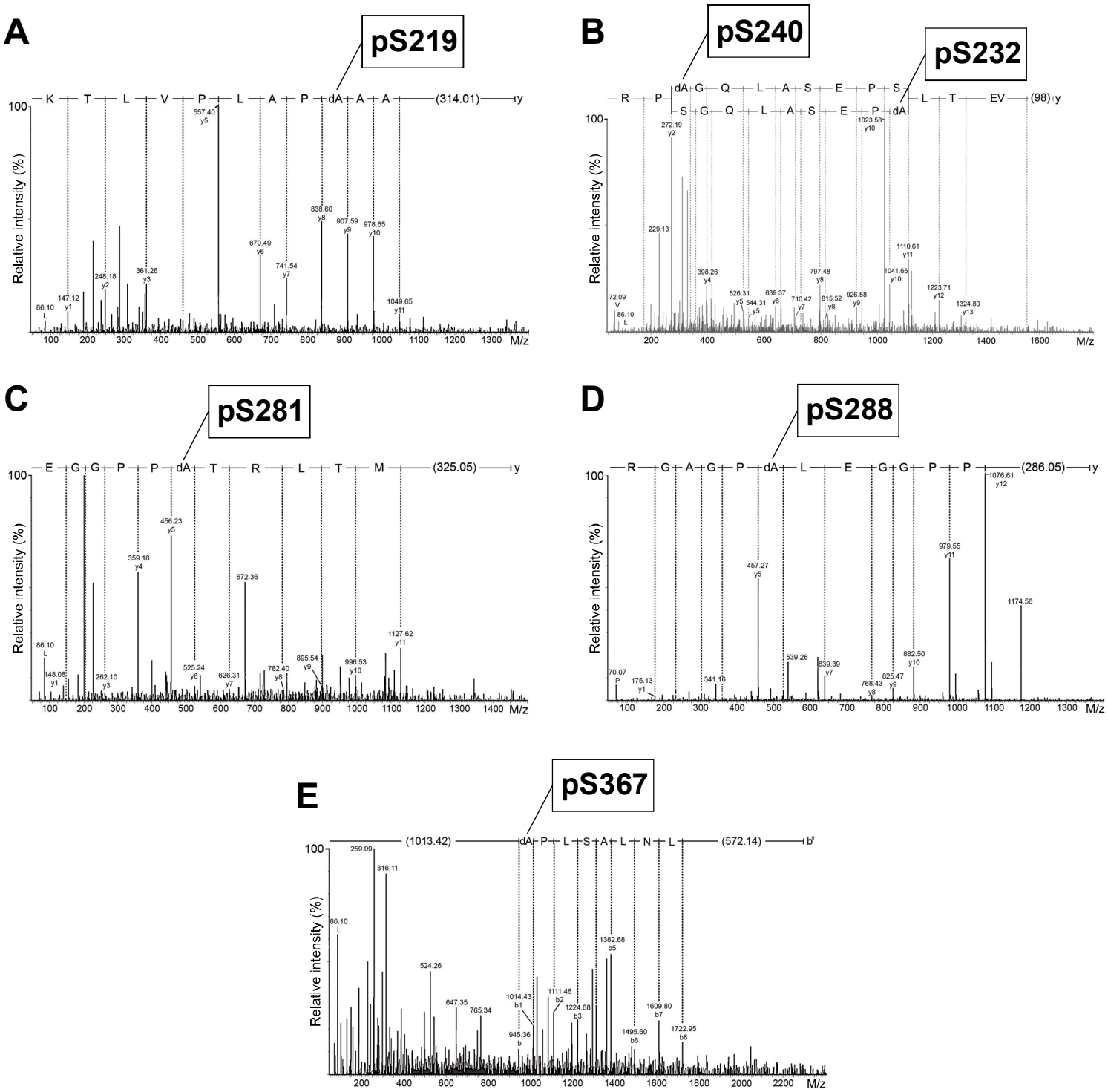

Supplemental Figure S2. **Identification of six proline-directed serine phosphorylation sites in Myc-FOXC2 by LC-MS/MS analysis.** MS/MS fragmentation spectra of phosphorylated tryptic (A,B,C,D) or GluC (E) peptides derived from Myc-FOXC2. Callouts indicate phosphorylated serine residues and their positions in the untagged protein. Dehydroalanine (dA) represents chemical signature left by the neutral loss of phosphoric acid from the phosphorylated serine residues.

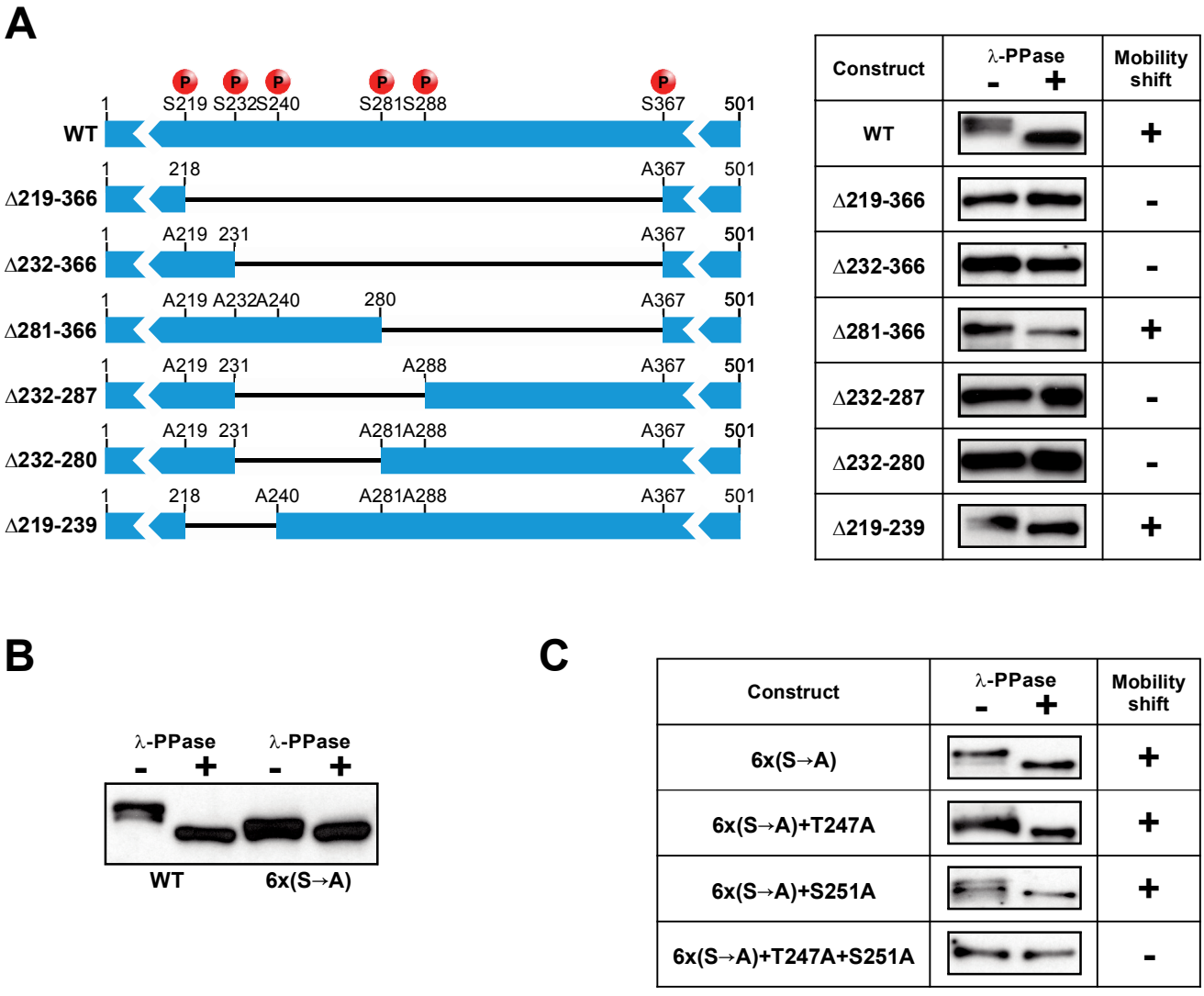

6x(S→A) = S219A+S232A+S240A+S281A+S288A+S367A

Supplemental Figure S3. **Identification of T247 and S251 phosphorylation sites in FOXC2 by deletion and site-directed mutagenesis.** (A) Systematic deletion mutagenesis of the phosphorylated domain in Myc-FOXC2. Positions of six phosphorylated serine residues identified by LC-MS/MS are shown as red spheres above the wild type (WT) protein sequence. These residues have been replaced by alanines (A219, A232, A240, A281, A288 and A367) in six deletion mutants shown below. The effects of λ-PPase treatment on the electrophoretic mobility of wild type Myc-FOXC2 and each deletion mutant are summarized in the table on the right. Two out of six deletion mutants exhibited electrophoretic mobility shifts upon enzymatic dephosphorylation, narrowing the phosphorylation site search to a stretch of amino acids from aa241 to 280. (B) Side-by-side comparison of phosphatase-induced changes in electrophoretic mobility of wild type Myc-FOXC2 and its mutant 6x(S→A), in which S219, S232, S240, S281, S288 and S367 were replaced by alanines. (C) Site-directed mutagenesis of two potential proline-directed phosphorylation sites (T247 and S251) between aa241 and 280. Simultaneous but not successive replacement of T247 and S251 with alanine, bringing the total number of alanine substitutions to eight, abolished the phosphorylation-dependent electrophoretic mobility shift of Myc-FOXC2. Shown are Western blots probed with anti-Myc antibody.

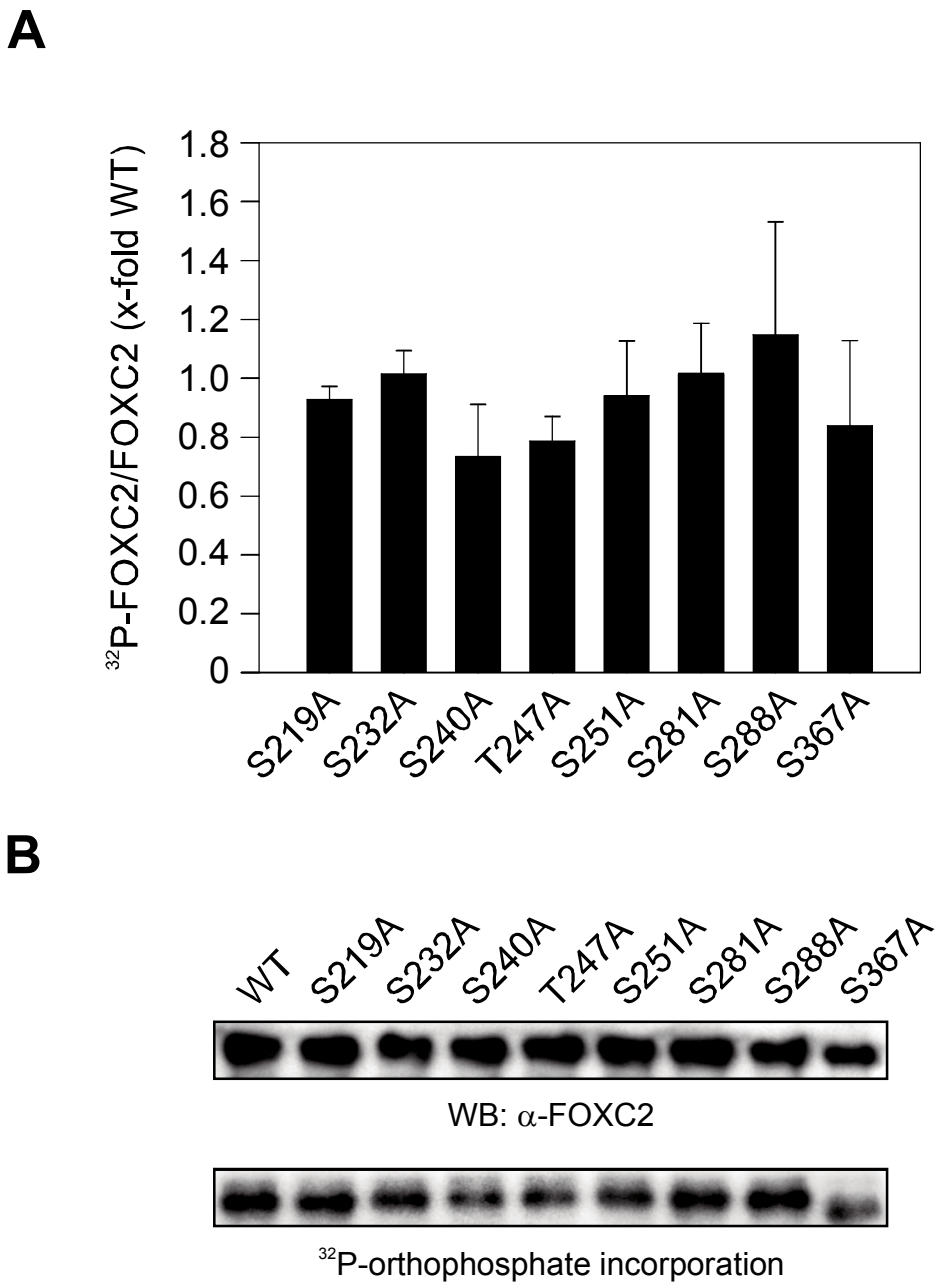

Supplemental Figure S4. **FOXC2 does not contain distinct primary and secondary phosphorylation sites.** (A) Eight individual phosphorylation site mutants of Myc-FOXC2, each having only one phosphorylated residue mutated to alanine, were assayed for metabolic incorporation of radioactive orthophosphate. The radiolabeled proteins were immunoprecipitated from cell lysates with anti-Myc antibody and analyzed by immunoblotting and autoradiography. The intensity of each radioactive band was quantitated by densitometry and normalized to the amount of immunoprecipitated protein. The data are presented as fold change relative to the level of radioactive orthophosphate incorporated into wild type (WT) Myc-FOXC2. Bars correspond to the mean of two independent experiments ± standard deviation. Note that none of the individual mutations alone caused a strong decrease in radioactive phosphate incorporation into FOXC2. (B) Representative immunoblot and autoradiogram.

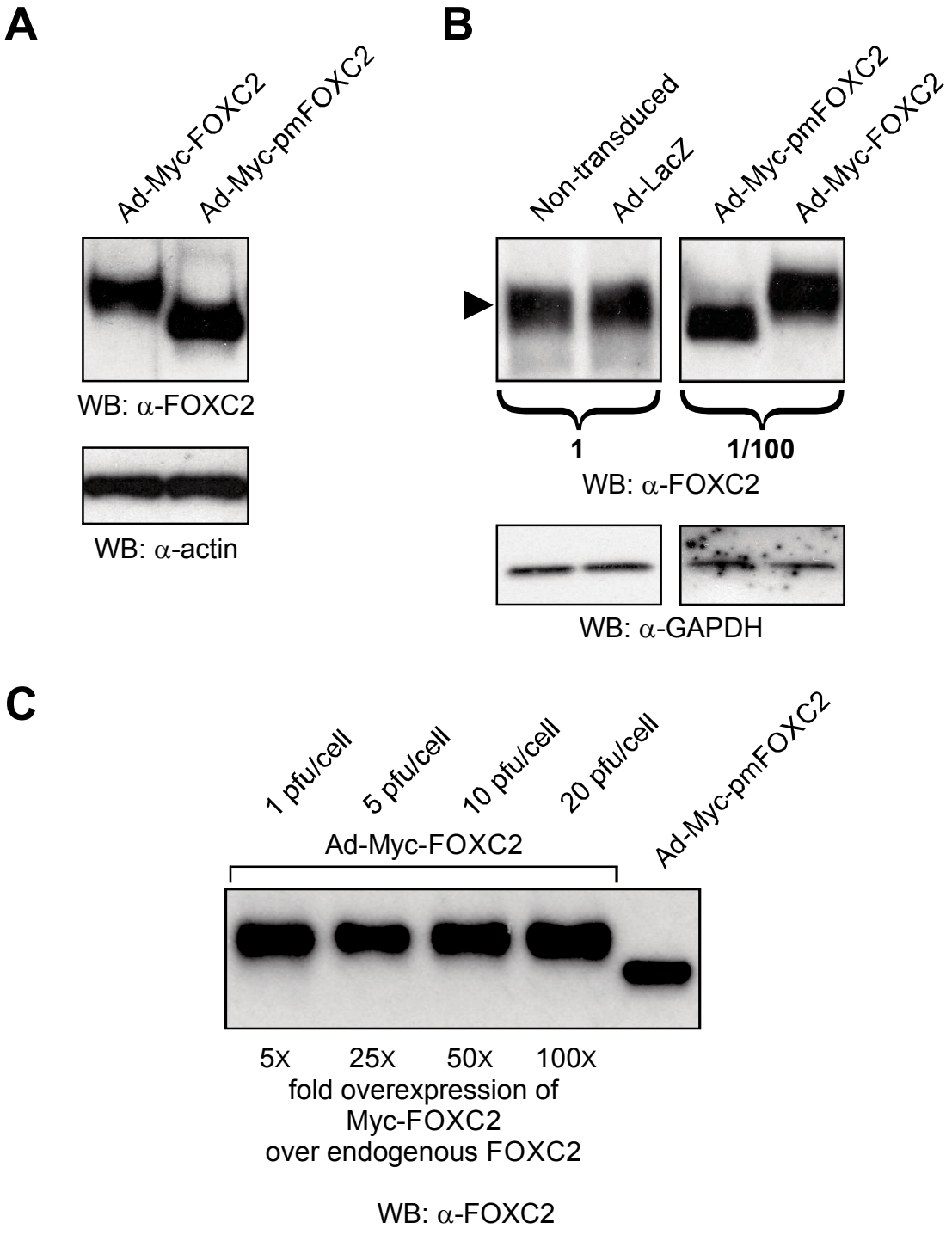

Supplemental Figure S5. **Immunoblot analysis of Myc-FOXC2 and Myc-pmFOXC2 expression in LECs.** (A) Myc-FOXC2 and Myc-pmFOXC2 are expressed at similar levels in LECs transduced with 20 plaque-forming units per cell (pfu/cell) of the corresponding recombinant adenoviruses. (B) Comparison of endogenous and exogenous FOXC2 expression levels in LECs. Lysates of LECs transduced with 20 pfu/cell of Ad-Myc-FOXC2 were diluted 100-fold to achieve band intensity similar to that of endogenous FOXC2. The position of endogenous FOXC2 is marked by an arrowhead. Note that Myc-FOXC2 has lower electrophoretic mobility than endogenous FOXC2 due to the extra 1.5 kDa coming from the Myc-tag. (C) Rising levels of FOXC2 expression in LECs have no impact on its electrophoretic mobility, suggesting that the phosphorylation status of FOXC2 is not significantly affected by its overexpression. Note the absence of FOXC2 mobility shift in cells transduced with increasing quantities of Ad-Myc-FOXC2. The amounts of cell lysates loaded on the gel were adjusted to produce FOXC2 bands of approximately equal intensity. Myc-pmFOXC2 was run in parallel as a control for mobility shift. Shown are Western blots of LEC lysates probed with anti-FOXC2, anti-actin or anti-GAPDH antibodies. In lane Ad-LacZ, LECs were transduced with recombinant adenovirus expressing an irrelevant gene, bacterial β-galactosidase.

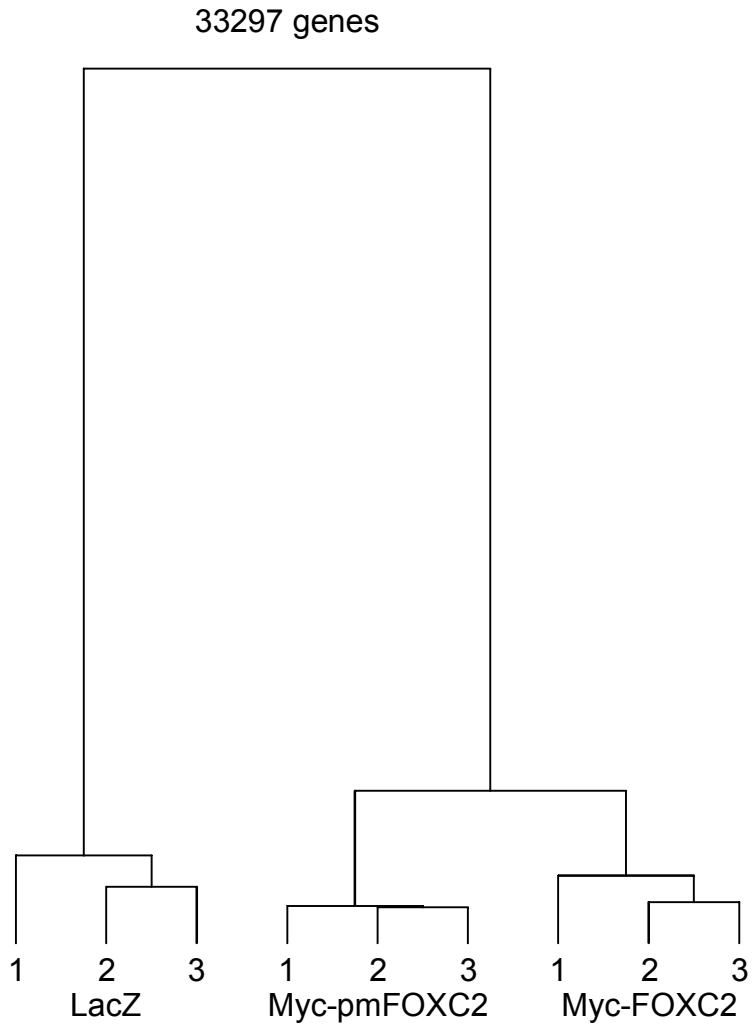

Supplemental Figure S6. **Dendrogram illustrating the hierarchial cluster analysis of microarray gene expression data.** The data were obtained from LECs overexpressing Myc-FOXC2, Myc-pmFOXC2 or a control protein, bacterial β-galactosidase (LacZ). Three biological replicates were performed for each experiment. Note that Myc-FOXC2 and Myc-pmFOXC2 form separate clusters.

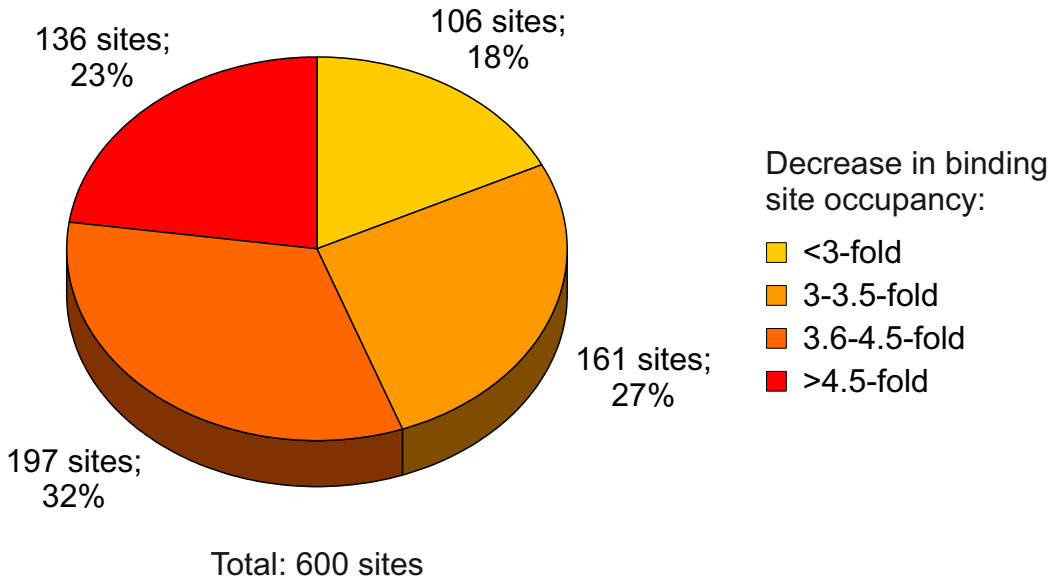

Supplemental Figure S7. **Loss of phosphorylation exerts variable inhibitory effects on FOXC2 recruitment to physiological binding sites in LECs.** The chart shows proportional distribution of the inhibitory effects across 600 phosphorylation-regulated binding sites enriched in Myc-FOXC2 over Myc-pmFOXC2 (p-value<10^{-5}) and overlapping with endogenous FOXC2 binding sites from Norrmén et al., 2009.

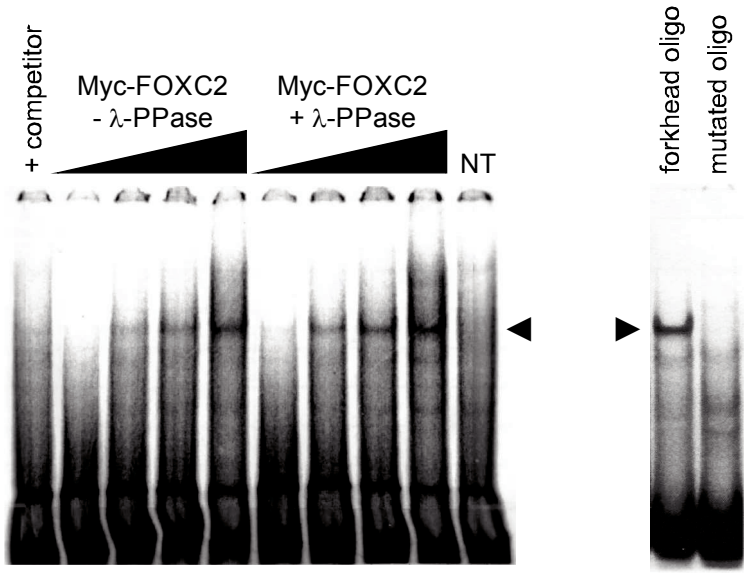

Supplemental Figure S8. **Dephosphorylation with λ-PPase does not affect the *in vitro* binding of Myc-FOXC2 to double stranded oligonucleotide bearing two forkhead consensus motifs.** We used electrophoretic mobility shift assay (EMSA) to determine whether the DNA binding activity of Myc-FOXC2 is reduced following treatment with λ-PPase. Increasing amounts of Ad-Myc-FOXC2-transduced cell lysates were treated (+) or not (-) with λ-PPase and incubated with radiolabeled dsDNA oligonucleotide 5'-GATCCTTAAGTAA-**GTAAACAAACA**AGATCCTTAAGTAA**GTAAACAAACA**AGATC-3' (only one strand is shown, forkhead consensus sequences are in bold and underlined). The resulting protein-DNA complexes were resolved by gel electrophoresis and visualized by phosphorimager analysis. Arrowhead indicates the position of specific Myc-FOXC2-DNA complexes. The binding specificity was confirmed by (a) competition EMSA using unlabeled dsDNA of the same sequence (left lane), (b) incubation of radiolabeled dsDNA with nontransduced cell lysate (lane NT), and (c) incubation of Ad-Myc-FOXC2-transduced cell lysates with radiolabeled oligonucleotide mutated in the consensus forkhead binding site (**TGGAACAAATA**, mutated nucleotides are highlighted in grey, right panel).

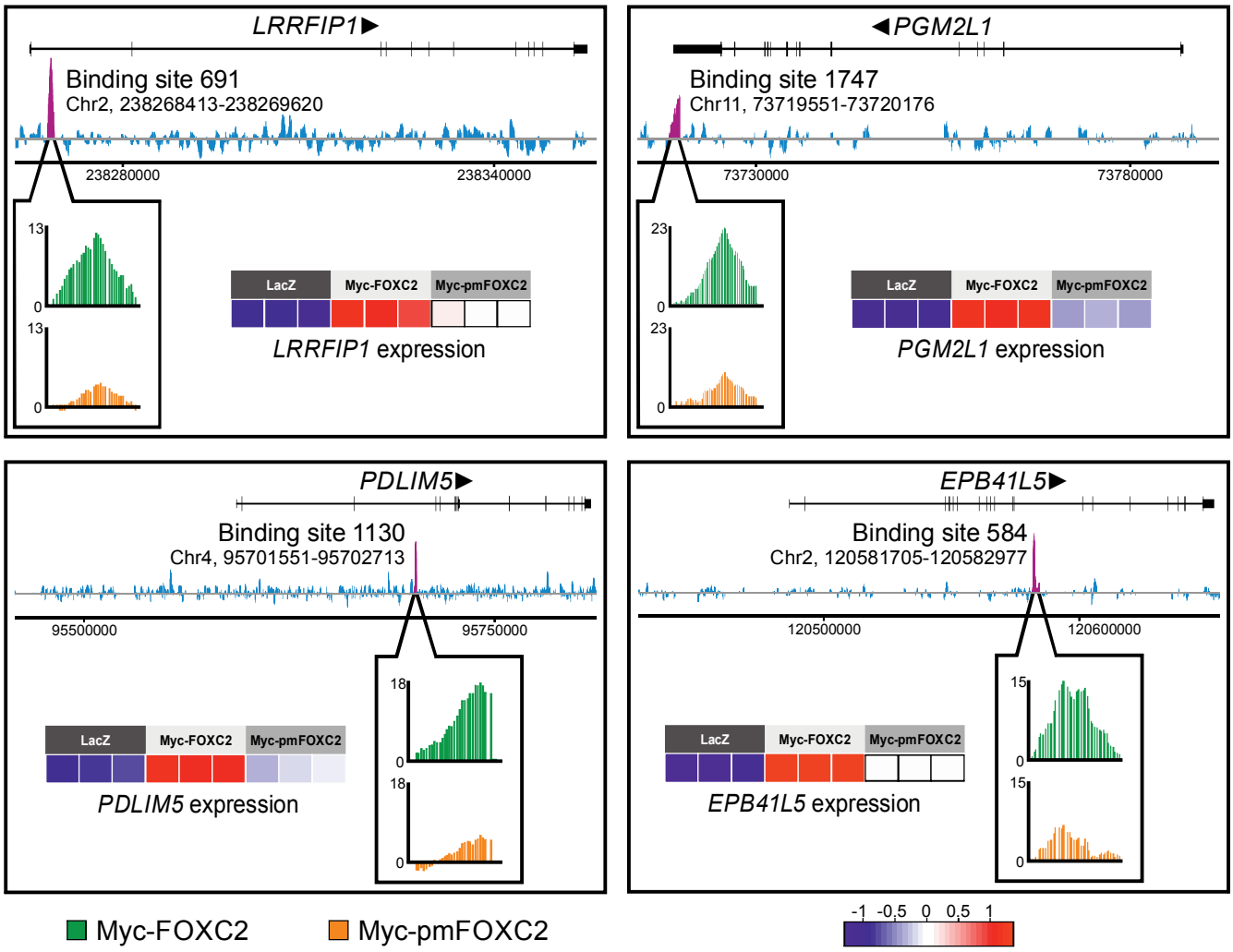

Supplemental Figure S9. **Loss of FOXC2 phosphorylation downregulates expression of putative direct FOXC2 target genes.** Shown is the correlation between the decreased FOXC2 recruitment to genomic binding sites in response to the loss of phosphorylation and the decreased transcriptional activation of the neighboring putative direct FOXC2 target genes. The positions of the genes are indicated at the top of each panel. Vertical lines, exons; horizontal lines, introns. For each gene, only one splice variant is shown. Arrowheads indicate the direction of transcription. Below are enrichment profiles of endogenous FOXC2. Purple peaks indicate FOXC2-enriched regions; their relative occupancies by Myc-FOXC2 and Myc-pmFOXC2 are shown in callout boxes in green and orange, respectively. Vertical axes represent MAT score. Endogenous FOXC2 binding sites are numbered as in Norrmén et al. (2009); genomic coordinates refer to the hg18 human genome assembly. Heat maps show the expression levels of putative direct FOXC2 target genes in iLECs transduced with Ad-LacZ, Ad-Myc-FOXC2 and Ad-Myc-pmFOXC2. Three biological replicates are shown for each experiment. Color key at the lower left corresponds to the arctan-transformed log2-fold change in gene expression. Blue denotes genes with relative decreased expression, red denotes genes with relative increased expression.

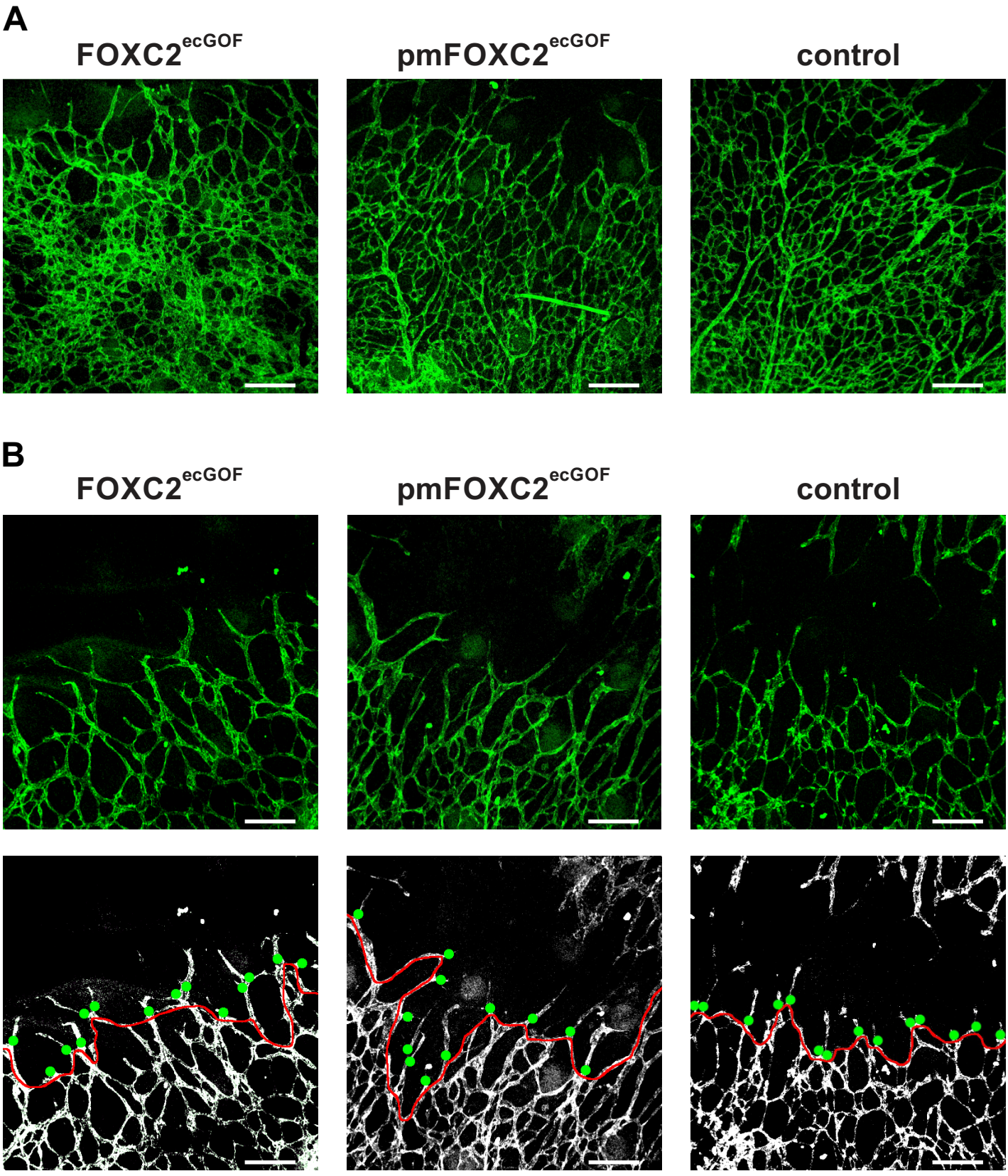

Supplemental Figure S10. **Overexpression of FOXC2, but not pmFOXC2, promotes vascular remodeling in maturing capillaries.** (A) Lower magnfication view of capillary plexus in the head skin of E15.5 embryos. Whole-mount staining for pan-endothelial marker CD31. Bar, 200 μm. (B) Example of images used for quantification of sprouting at the vascular front in FOXC2^{ecGOF}, pmFOXC2^{ecGOF} and control embryos. Green dots indicate sprouting endothelial cells, and red line outlines the angiogenic front as described in Pitulescu et al., 2010. Bar, 145 μm.

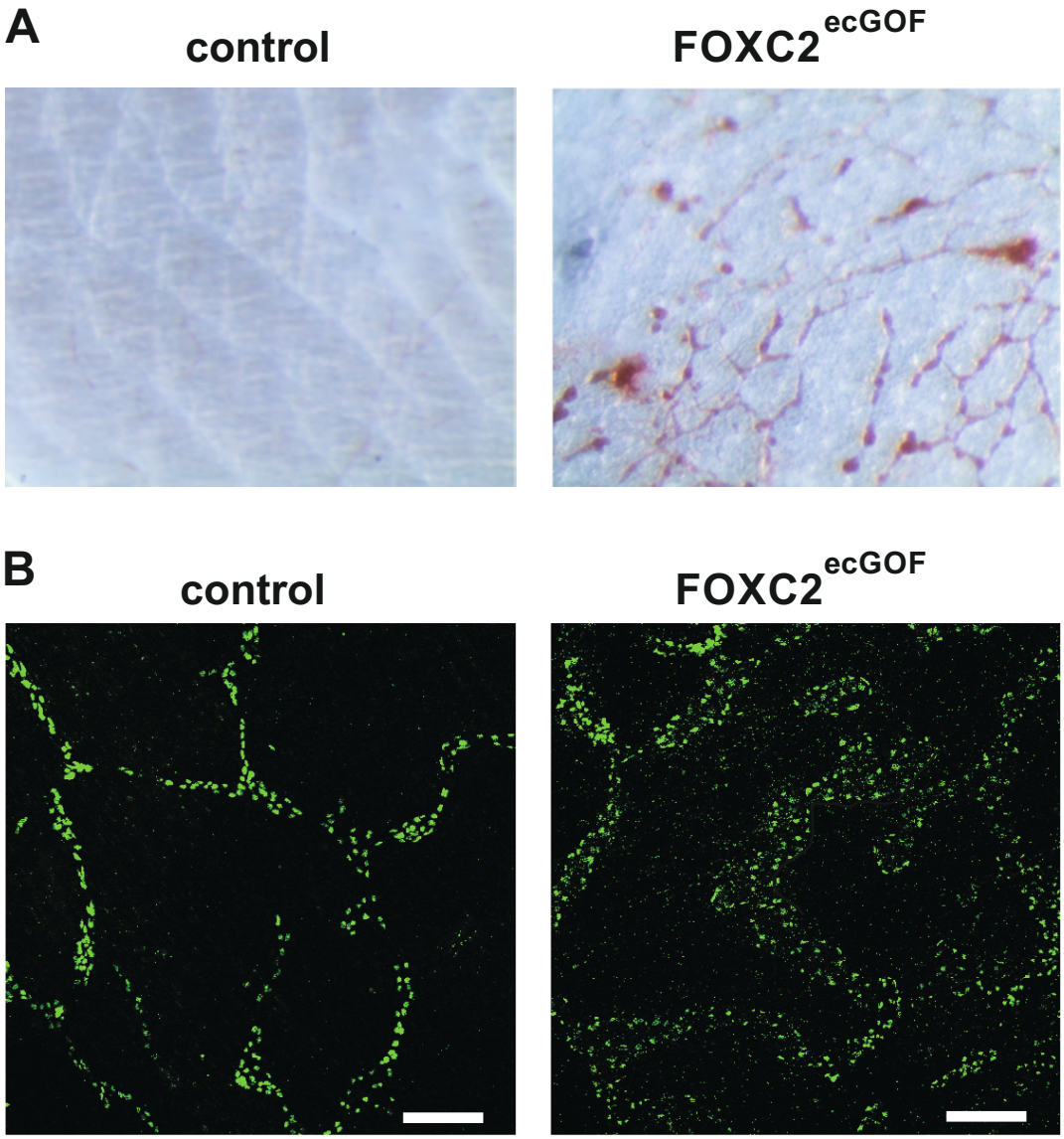

Supplemental Figure S11. **Example of blood-filled lymphatic vessels in FOXC2^{ecGOF} embryos.** (A) Dorsal skin of E16.5 control and FOXC2^{ecGOF} embryo. (B) Whole mount staining of control or blood-filled dermal lymphatic vessels in FOXC2^{ecGOF} mice. Immunofluorescent staining for PROX1 (green) at E16.5. Bar, 150 μm.

Supplemental Tables

Supplemental Table S1. **Masses, relative intensities and positions of tryptic peptides derived from Myc-FOXC2 treated (+) or not (-) with lambda protein phosphatase (λ-PPase).** Phosphopeptides are marked in red. Peptide masses are given in daltons (Da); amino acid numbering is the same as in the untagged protein.

Myc-FOXC2 - λ-PPase		Myc-FOXC2 + λ-PPase			
Observed m (Da)	Relative intensity	Observed m (Da)	Relative intensity	Theoretical m (Da)	Position (amino acids)
1505,707	4654	1505,687	1690	1505,736	-8-4
2533,203	1647	2533,180	949	2533,211	5-26
2775,128	2785	2775,112	1433	2775,183	27-54
1602,736	96	1602,720	45	1602,768	55-68
2247,006	62	2246,990	27	2247,196	73-92
3353,744	179	3353,686	143	3353,667	111-138
987,474	61	987,465	30	987,488	114-121
2141,174	51	2141,140	20	2141,104	122-139
2498,055	160	2498,025	93	2498,085	143-163
1649,747	550	1649,722	276	1649,909	168-180
1567,733	115	1567,721	62	1567,831	172-184
1244,672	591	1244,649	262	1244,687	181-192[a]
1244,632	553	1244,629	238	1244,651	193-205[a]
1701,846	71	1701,829	35	1701,868	193-209
3401,827	102	3401,768	204	3401,912	210-242
3481,795	88	3481,777	58	3481,878	P + 210-242
1282,705	806	1282,679	403	1282,713	215-227
1362,655	237	1362,643	65	1362,679	P + 215-227
1569,773	933	1569,750	789	1569,799	228-242
1649,747	550	1649,722	276	1649,766	P + 228-242
1729,712	71	1729,689	13	1729,732	2P + 228-242
3655,683	1373	3655,606	1907	3655,769	243-279
1281,611	474	1281,609	1816	1281,631	280-293
1361,584	596	1361,570	67	1361,597	P + 280-293
1441,548	68			1441,563	2P + 280-293
3954.878[b]	1078	3954.831[b]	975	3956,937	294-334
919,388	48	919,369	16	919,397	452-458
2522,170	60	2522,133	9	2522,206	459-482
832,435	109	832,407	109	832,444	483-489
1417,579	84			1417,597	490-501

[a] peptides identified based on retention times
[b] reduced peptide mass likely due to internal disulfide bond

Supplemental Table S2. **Masses, relative intensities and positions of Glu-C peptides derived from Myc-FOXC2 treated (+) or not (-) with lambda protein phosphatase (λ-PPase).** Phosphopeptides are marked in red. Peptide masses are given in daltons (Da); amino acid numbering is the same as in the untagged protein.

Myc-FOXC2 - λ-PPase		Myc-FOXC2 + λ-PPase			
Observed m (Da)	Relative intensity	Observed m (Da)	Relative intensity	Theoretical m (Da)	Position (amino acids)
1462,763	237	1462,759	268	1462,685	-12- (-1)
2368,236	776			2368,170	0-21
2649,213	1837	2649,203	30	2649,138	22-46
2331,349	64			2331,255	70-90
1013,557	30	1013,546	104	1013,508	105-111
2037,086	342			2037,014	112-128
2792,620	387	2792,633	14	2792,562	158-179
2956,597	6665	2956,594	5403	2956,551	180-208
1129,727	56	1129,716	41	1129,670	207-216
1822,071	629	1822,066	600	1822,008	217-234
1902,058	2277			1901,974	P + 217-234
1982,006	854			1981,941	2P + 217-234
2239,132	969	2239,112	6255	2239,071	235-258
2319,116	1128	2319,081	3499	2319,037	P + 235-258
1502,780	4034	1502,771	1146	1502,726	259-273
1371,719	953	1371,703	2807	1371,682	274-286
1451,701	911			1451,648	P + 274-286
2232,184	1140	2232,164	445	2232,101	357-379
2312,120	4496			2312,067	P + 357-379
1202,628	8285	1202,624	6248	1202,586	453-462

Supplemental Table S3. **Gene expression signature associated with the loss of FOXC2 phosphorylation in primary LECs.** Shown are 467 genes differentially expressed (>1.5 fold difference, FDR<0.01) between LECs transduced with Ad-Myc-FOXC2 and Ad-Myc-pmFOXC2 (see text for detailed gene selection criteria). Names of genes upregulated or downregulated more than 2-fold are highlighted in orange and purple, respectively. Putative direct FOXC2 target genes regulated by FOXC2 phosphorylation are marked with an asterisk (*). For these genes, downregulated expression (>1.5 fold change, FDR<0.01) in response to the loss of FOXC2 phosphorylation correlated with the decrease in FOXC2 recruitment to nearby (within 300 kb) phosphorylation-regulated binding site(s). Such sites are defined as enriched in Myc-FOXC2 over Myc-pmFOXC2 (p-value<10^{-5}) and overlapping with physiological FOXC2 binding sites enriched in endogenous FOXC2 over IgG control (FDR<0.001; Norrmén et al., 2009).

Genes downregulated in response to the loss of FOXC2 phosphorylation in primary LECs		Genes upregulated in response to the loss of FOXC2 phosphorylation in primary LECs	
ACSL4	*ME2*	***ABCA4***	***ITGB3***
ACTR6	*MEGF9*	***ABHD2***	*KDELR3*
AGTPBP1	***MGAT4A***	***ACACA***	***KIAA0101***
ANKRD1	*MMP16*	***ACAD10***	*KIAA1279*
ANKRD5	*MORC4*	*ACSS2*	*LAMA4*
ANLN	***MPZL3***	***AGPAT5***	*LDHA*
APAF1	***MRC1***	*ALDH1A1*	*LGALS3BP*
APOL4	*MTBP*	*ALDH7A1*	*LOC286297*
AREG	*MYCT1*	***ALDOC***	*LPCAT3*
ARHGDIB	*NCAPG*	***AMIGO3***	*MAP1B*
ARL13B	*NDFIP2*	***ANAPC1***	***MATN2***
ASPM	***NEO1***	*AP1S3*	***MBOAT4***
B3GNT2	***NET1***	*AP4S1*	***MBTD1***
B4GALT4	***NHEDC2***	***AS3MT***	***METTL7A***
BAIAP2L1	*NRG3*	*ATP6V1A*	***MLH3***
BAZ2B	***NSBP1***	*BPHL*	***MMP10***
BCL6	***NUF2***	***BTN3A1***	*MORN3*
BLZF1	*NUSAP1*	***BTN3A2***	*MPHOSPH9*
BMPR1A	*OBFC2A**	***C11orf83***	*MTHFD2*
BNC1	***OVOS***	*C12orf55*	*MX1*
BRWD3	***OVOS2***	***C16orf73***	***MYLK4***
BTAF1	***PAIP2B***	***C17orf57***	*N4BP2L1*
BTBD3	*PCDH12*	***C1R***	***NAAA***
*C10orf118**	*PDLIM5**	***C4orf49***	*NEFH*
C11orf63	*PECAM1*	*C5orf4*	*NFKB2*
C12orf4	***PGM2L1****	*C6orf106*	***NRIP2***
C18orf19	*PHF7*	*C7orf23*	*NUCB2*
C18orf54	*PHKA1*	***CARD8***	***OAS1***
C1GALT1	*PIK3CA*	*CCBL2*	*OAS3*
C21orf119	*PIK3R3*	***CCNE2***	*OAT*
C22orf28	*PIP5K3*	***CCRL1***	***OGN***
C2orf44	*PKHD1L1*	***CD36***	***P2RY5***
*C3orf26**	*PLAG1*	***CENPF***	*PAPSS2*
C4orf18	***PLEK***	*CEP110*	*PBX3*
C6orf173	*PLEKHF2**	*CGREF1*	*PDE4B*
*CA5B**	*PLS1*	*CHAC1*	*PFN2*
CABYR	*PLTP*	***CHAC2***	***PLA1A***
CCDC103	*POP1*	***CHRNA6***	***PLA2G10***

CCDC134	POSTN	CLDN7	PLAU
CCDC14	PPM1A	CLEC1A	PLAUR
CCDC80	PPP3CC	CLU	PLCE1
CCL2	PRDM1	CP	PLD6
CCNA1	PRKAA2	CPB1	PPAT
CCNA2	PRPSAP2	CSGALNACT1	PRICKLE1
CCNB2	PRUNE	CTDSPL	PSAT1
CDC2	PTGS2	CXCL16	PSEN2
CENPQ	PTPRK	CXorf23	PSPH
CHIC2	PUS10	DCXR	PSTPIP2
CHMP2B	QPCT	DENND2C	PTPRB
CLIC2	RALGPS2	DNAJC12	PTPRS
COPS8	RASSF2	DOCK9	PYCR1
COX16	RASSF9	DPP4	RACGAP1
CPEB4*	RB1CC1	EAF2	RARB
CREB5	RBM19	EBP	RCN3
CRHR1	RBM27	EIF2B3	RDH12
CSGALNACT2	RCAN3	ELA2A	RFTN2
CSNK1G3*	REXO2	ENTPD5	RNASEN
CTAGE4	RFPL4A	ERG	RNF144B
CTGF	RICTOR	ESM1	RUFY3
CYB5R4	RIOK1	EVI2B	SAMD9
CYLD	RLF	FAM122B	SAMHD1
CYP4X1	RNGTT	FAM177A1	SCNN1B
DCP1A	RNMT	FAM49A	SCNN1G
DDX52	RPAP3	FANCD2	SDPR
DENND1B	RPGR	FECH	SEPP1
DGKA	RPS6KA5	FIGF	SERPINB1
DHX8	RRN3	FLJ11235	SHANK3
DICER1	RRP12	FLVCR2	SLC16A6
DIRC2	RSRC1	FNDC5	SLC1A1
DLGAP5	RTF1	FREQ	SLC25A30
DNAJC24	RTN3	FRRS1	SLC25A4
DONSON	S100A16	FZD4	SLC31A1
DUSP14	SAV1	GAB3	SLC44A3
DUSP18	SCN3B	GCNT1	SNX22
EBNA1BP2	SDCCAG10	GK	SRXN1
EDN1	SEMA3D	GLDC	SYNPO
EFCAB5*	SERPINI1	GNG7	SYTL4
ELTD1	SHOC2	GNPNAT1	TBC1D4
EMP1	SIPA1L2	GOLM1	TCTN2
EPB41L5*	SLC19A2	GOLPH3L	TGFB3
ERRFI1	SLC25A21	GPD1L	TLR3
ETS2	SLC26A4	GPER	TM4SF1
ETV4	SLC35B3	GPR160	TMCO7
EVI5	SLC39A12	GRHL1	TMEM20
EZH2	SLC41A2	HBEGF	TMEM56
FAM100B	SLC5A6	hCG_2045899	TNFSF10
FAM114A1	SLC7A8	HCP5	TSPAN7
FAM126B	SLFN5	HFE	TWSG1
FAM172A	SLU7	HPRT1	USP18
FAM98B	SMC2	HSPA2	USP39
FANCI	SNORD50B	IFI6	USP41
FANCL	SNRPN//SNORD115	IFIT1	WEE1
FBXL20	-11	IFIT2	XPO4
FBXO42	SNRPN//SNORD115	IFIT3	ZNF114
FHL2*	-26	IGJ	ZNF608

FMR1 *FRMD5* *GARNL1* *GBP2* *GCA* ***GFRA1**** ***GIMAP5*** *GLRB* *GLT8D3* *GMFG* ***GNG2*** *GPN3* *HERC5* *HHIP* *HIST1H2BK* *HMCN1* *HMMR* *JHDM1D* *KATNA1* *KCTD9P2* *KIAA0256* *KIAA0895* *KIAA1107* *KIF11* *KIF20A* ***KLHL4*** ***KLHL7*** ***LCA5*** *LIFR* *LMTK2* *LOC171220* ***LOC643837*** *LOC727963* *LOC729927* ***LPHN2*** *LRRC28* ***LRRFIP1**** *LSG1* *MAK10* *MAP3K7IP3* *MAP9* *MAPKBP1* *MARCH8*	*SNX7* *SP110* ***SPAG5*** *SPOPL* *ST8SIA4* *STAT2* *STAT3* ***STON1-GTF2A1L*** *STXBP3* *SULT1B1* *SYT11* ***TCP11L2*** ***TDRKH*** *TEX10* *TGFA* *THBS1* ***TLE4*** ***TMEM154*** ***TMLHE*** *TNFRSF10D* *TOM1L1* *TPR* ***TSHZ2*** *TTC18* ***TTLL4*** *TUBA1A* *UBTD2* *UBXN7* *UHRF1BP1L* *USP53* *UTP6* *VAMP1* *WBP4* *WDR44* *WDR63** *WDR91* *ZFPM2* *ZMPSTE24* *ZNF410* *ZNF490* *ZNF611* *ZNF654* *ZNF711* *ZRANB1* *ZW10*	*IKBKAP*	

Supplemental References

Norrmén, C, Ivanov, KI, Cheng, J, Zangger, N, Delorenzi, M, Jaquet, M, Miura, N, Puolakkainen, P, Horsley, V, Hu, J, Augustin, HG, Yla-Herttuala, S, Alitalo, K, Petrova, TV. 2009. FOXC2 controls formation and maturation of lymphatic collecting vessels through cooperation with NFATc1. J Cell Biol **185:**439-57.

Pitulescu, ME, Schmidt, I, Benedito, R, Adams, RH. 2010. Inducible gene targeting in the neonatal vasculature and analysis of retinal angiogenesis in mice. Nature protocols **5:**1518-34.